

Innermost structure and near-infrared radiation of dusty clumpy tori in active galactic nuclei

Toshihiro Kawaguchi

Dept. of Physics and Information Science, Yamaguchi University, Yoshida 1677-1,
Yamaguchi 753-8512, Japan

Abstract

The dusty clumpy torus surrounds the central black hole (BH) and the accretion disk in active galactic nuclei, and governs the growth of super-massive BHs via gas fueling towards the central engine. Near-infrared (NIR) monitoring observations have revealed that the torus inner radius is determined by the dust sublimation process. However, the observed radii are systematically smaller than the theoretical predictions by a factor of three.

We take into account the anisotropic illumination by the central accretion disk to the torus, and calculate the innermost structure of the torus and the NIR time variability. We then show that the anisotropy naturally solves the systematic discrepancy and that the viewing angle is the primary source to produce an object-to-object scatter of the NIR time delay. Dynamics of clumps at the innermost region of the torus will be unveiled via future high-resolution X-ray spectroscopy (e.g., Astro-H).

1 Introduction

Active galactic nuclei (AGNs) are powered by gas accretion onto supermassive black holes (BHs) at the center of each galaxy. A variety of observations suggest that the accretion disk and the BH are surrounded by an optically and geometrically thick torus (e.g., [37], [3]). Since the torus potentially plays a role of a gas reservoir for the accretion disk, its nature, such as the structure, the size and the mass, has long been investigated ([29], [30],[10], [11], [8]).

A large geometrical thickness of the torus revealed by various observations ([2], [31], [39], [33]) indicates that numerous dusty clumps, rather than a smooth mixture of gas and dust, constitute the torus with a large clump-to-clump velocity dispersion ([22]). Temperature of clumps is less than a critical temperature $T_{\text{sub}} \sim 1500$ K above which dust grains are sublimated ([4]).

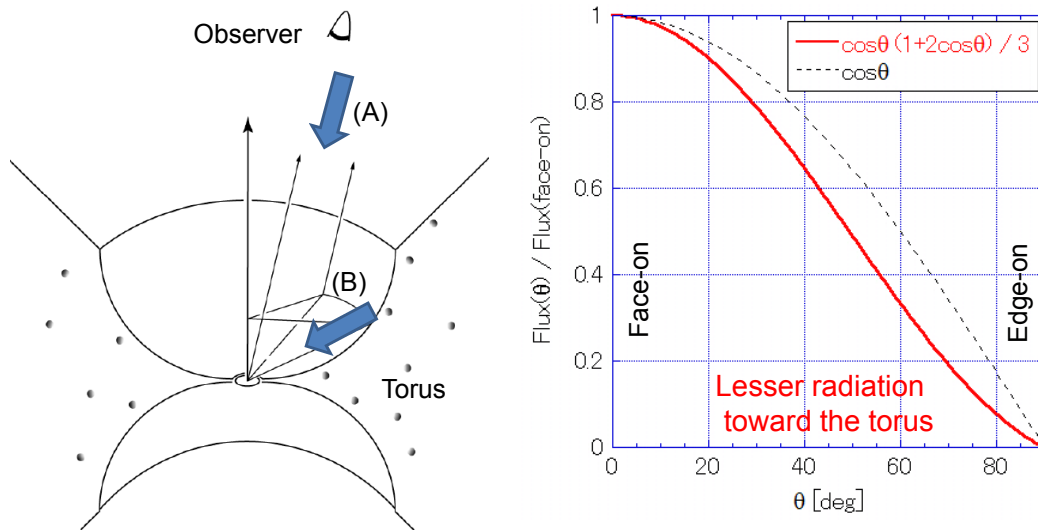


Figure 1: Left: (A) The inclination angle at which we observe the disk in type-1 AGNs is systematically different from (B) the angle at which an aligned torus observes the disk [18]. Right: Flux changes with the direction [19]. We must be aware that the flux towards the torus (B) is much weaker than that to the observer (A).

Based on the energy balance of the clump closest to the BH, Barvainis ([4]) derived the innermost radius of the torus (dust sublimation radius, denoted as $R_{\text{sub},0}$ in this study):

$$R_{\text{sub},0} = 0.13 \left(\frac{L_{\text{UV}}}{10^{44} \text{ erg s}^{-1}} \right)^{0.5} \left(\frac{T_{\text{sub}}}{1500 \text{ K}} \right)^{-2.8} \left(\frac{a}{0.05 \mu\text{m}} \right)^{-0.5} \text{ pc}, \quad (1)$$

where L_{UV} and a are UV luminosity and the size of dust grains, respectively.

Indeed, Near-infrared (NIR) emission from type-1 AGNs lags behind optical variation by an order of $R_{\text{sub},0}/c$ ([6], [12], [13], [25], [28], [24], [35]). Moreover, the luminosity dependency of the time lag also coincides with the theoretical prediction as $\propto L_{\text{UV}}^{0.5}$ ([36]). However, the NIR-to-optical time lag is systematically smaller than the lag predicted from Equation (1) by a factor of $\sim 1/3$ ([27], [21], [26]). To tackle with this conflict, Kawaguchi & Mori ([18]) pointed out that the illumination by an optically thick disk is inevitably anisotropic, which is a fact missing in deriving Equation (1). There is a systematic difference between (A) the inclination angle at which we observe the disk in type-1 AGNs and (B) the angle at which an aligned torus observes the disk (Figure 1, left). The effects of the anisotropic illumination naturally resolve the puzzle of the systematic deviation of a factor of $\sim 1/3$ ([18]).

2 Anisotropic Emission of Accretion Disk

Radiation flux (F) from a unit surface area of the disk toward a unit solid angle at the polar angle of θ decreases with an increasing θ as follows:

$$F \propto \cos \theta (1 + 2 \cos \theta). \quad (2)$$

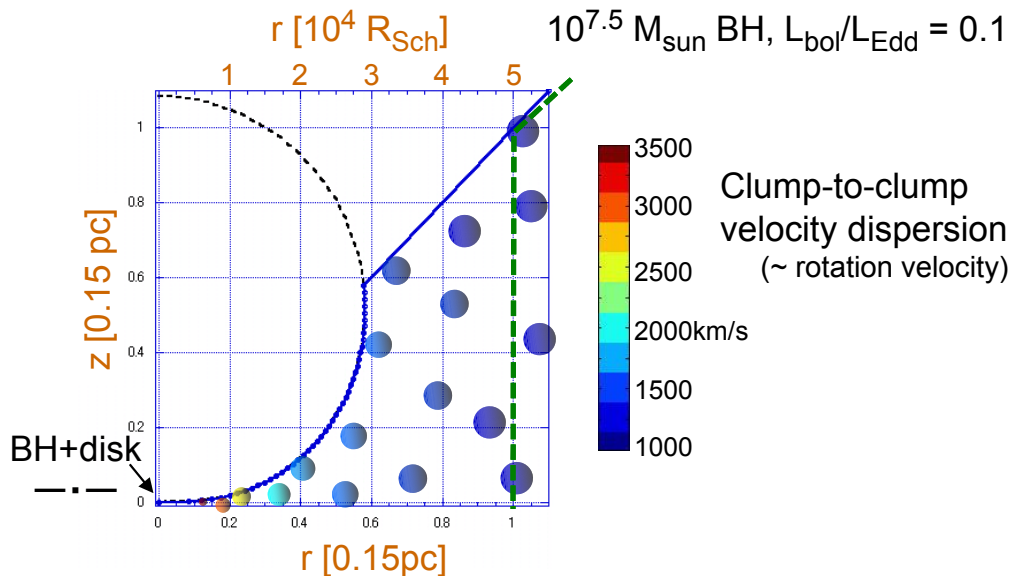


Figure 2: Inner region of the torus in the cylindrical coordinates (r, z) [18]. At the left-bottom corner, let us suppose that there are the central BH and the accretion disk. Thick blue solid curve indicates the edge of the torus, with the opening angle of the torus assumed to be 45 deg. On the right-hand side of the line, the temperatures of clumps are below the dust sublimation temperature. If an observer assumes that the disk illumination is isotropic, then he/she would expect the torus inner edge at $R_{\text{sub},0}$ (thick, green dashed line). Units of the scale (in pc and Schwarzschild radius R_{Sch}) are computed for a $10^{7.5} M_{\odot}$ BH, with $L_{\text{bol}}/L_{\text{Edd}}$ of 0.1 and L_{bol} of $\sim 3L_{\text{UV}}$. Different colors of clumps indicate the clump-to-clump velocity dispersion of the order of the rotational velocity ~ 1000 km/s. Temperature of clouds are less than or equal 1500 K, corresponding to ~ 4 km/s. The actual size of clumps are expected to be $\sim 10^{-3}$ of the distance to the BH, but drawn with much bigger sizes here for illustration purposes.

Therefore, an accretion disk emits lesser radiation in the direction closer to its equatorial plane (i.e., larger θ ; [23], [34]; Figure 1, right). (Relativistic effects, such as light bending near the BH, unlikely alter this anisotropy drastically.) Thus, the assumption of isotropic emission from accretion disks (e.g., eq.1) obviously overestimates the radiation flux toward the torus, and therefore overestimates the torus inner radius.

3 Inner Structure of Dusty Torus

We determine the inner edge of the torus so that the temperature of a clump (at the irradiated surface) equals to the sublimation temperature at the edge. As mentioned above, radiation flux from the accretion disk varies with the polar angle θ . Thus, the sublimation radius of the torus is also a function of θ , which is indicated by $R_{\text{sub}}(\theta)$. Although various grain sizes result in the sublimation process occurring over a transition zone rather than a single distance

([26]), we employ a sharp boundary for simplicity.

Figure 2 shows the calculated structure of the innermost region of the torus. The central BH and the accretion disk on the $z = 0$ plane are located at the origin of the coordinate axes (at the left-bottom corner). The actual size of clumps are expected to be $\sim 10^{-3}$ of the distance to the BH ([38], [15], see Appendix of [19]), but drawn as if they are much bigger for illustration purposes in this figure.

It turns out that (i) the torus inner edge is located closer to the central BH than suggested by previous estimations (eq. 1) and that (ii) the structure of the edge is concave/hollow. Moreover, (iii) $R_{\text{sub}}(\theta)$ decreases down to $0.1 \times R_{\text{sub},0}$ at $\theta = 88.5\text{deg}$. This radius coincides with the outermost radius of AGN accretion disks, which is determined by the onset of radial self-gravity of the disk (see [20]). Our result indicates that there is no gap between the torus and the disk.

4 Transfer Function

The innermost radius of the torus discussed above cannot be spatially resolved even in the coming decade. Thus, observations of time variability will continue to be powerful tools to explore the innermost structure of the torus. In this section, we calculate the time variation of NIR emission in response to a δ -function like variation of the irradiation optical/UV flux [the transfer function $\Psi(t)$].

To calculate $\Psi(t)$ for the clumpy torus, we consider the following items; (1) the optical path, (2) NIR emissivity of the torus inner region as a function of θ and (3) anisotropic emission of each clump. (4) We also include the effect of the torus self-occultation (i.e., absorption of NIR emission from a clump by other clumps on the line of sight). While the torus self-occultation is a minor effect for a typical type-1 AGN, it plays a significant role for inclined viewing angles, thick tori and misaligned tori.

Our calculation results explain the observed properties of the existing data (e.g., lag- L relations), and present theoretical predictions that will be tested observationally in the future. Details are given in [19]. Below, we show some examples of our calculation results shortly.

4.1 Viewing angle dependency

Figure 3 (left panel) shows the transfer functions for various viewing angles θ_{obs} , from an exactly pole-on geometry ($\theta_{\text{obs}} = 0\text{deg}$) to inclined viewing angles. With a large θ_{obs} ($\approx 40\text{--}44\text{deg}$), the line of sight grazes the upper boundary of the torus, which would correspond to the situation in type-1.8/1.9 AGNs.

In order to compare our results with the observed data more directly, the t_{delay} v.s. L_{UV} diagram is drawn in Figure 3 (right panel). Our loci for various θ_{obs} well cover the observed scatter. Namely, our model explains not only the systematic shift (by a factor of 3) on average, but also the scatter around the regression line.

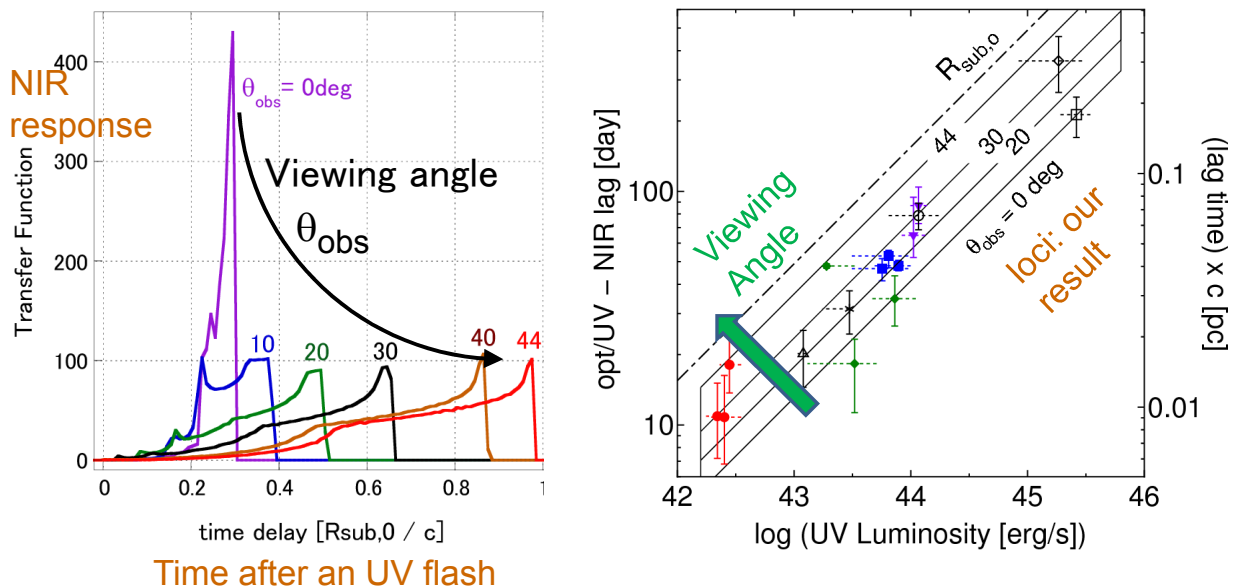


Figure 3: Left: Transfer functions for various viewing angles θ_{obs} , from a face-on view (purple) to intermediate type-1 cases (orange and red) [19]. The time delay appears longer for more inclined angles. Right: Our results (loci) on the time delay v.s. UV luminosity plane. Observed points are taken from [36], and covered well by our calculational results.

4.2 Accretion rate dependency

When the accretion rate exceeds the Eddington rate ($\approx 16L_{\text{Edd}}/c^2$), an optically thick advection-dominated accretion flow (a slim disk) appears ([1]). Since super-Eddington disks are geometrically thick ([1]), they cannot illuminate the directions near their equatorial plane by the disk self-occultation ([9]). Moreover, the observed data do not support the concept of Eddington-limited accretion ([7]). Thus, a strong anisotropy of the disk emission, such as Equation (2) and the disk self-occultation, is required to allow gas infall to super-Eddington accreting sources.

As discussed in [18], some AGNs with presumably super-Eddington accretion rates show the weak NIR emission (Ark564, TonS180, J0005 and J0303; [32], [20], [16]; see, however, [14]). Observationally, it is controversial whether high Eddington ratios are related to the weak NIR emission or not. Therefore, we here briefly summarize what are the expected behaviours from the theoretical sides ([19]).

We deduce the disk thickness at the Far-UV emitting region, based on the work by [17]. Although more detailed calculations of the accretion disk are possible (e.g., magnetohydrodynamical simulations rather than the α -description for the viscosity as used in [17]), it is a natural consequence that the disk puffs up as the accretion rate increases irrespective of calculational methods. We do not think that such time consuming calculations of the disk have scientific gains here.

Larger accretion rates make the disk thicker and the shade of the disk itself larger.

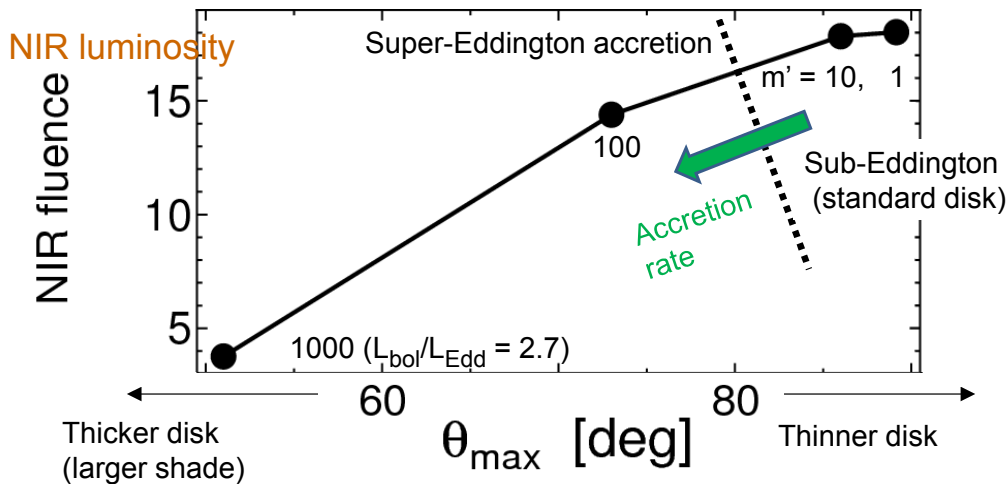


Figure 4: NIR fluence (an integration of the transfer function over time) as a function of the disk thickness (with θ_{\max} being the angle at the disk surface measured from the rotational axis towards the midplane at 90 deg) [19]. As the accretion rate \dot{M} (where \dot{m} represents \dot{M} in the unit of L_{Edd}/c^2 , with \dot{m} of 16 producing the Eddington luminosity L_{Edd}), the disk shade becomes large. Then, the expected NIR flux for the cases with high accretion rates (e.g., $\dot{m} = 1000$, shining at $2.7L_{\text{Edd}}/c^2$, see [17]) reduces down to $\sim 1/5$ of the NIR flux with sub-Eddington accretion rates.

Thus, the NIR fluence becomes small as the accretion rate increases. This is consistent with the weakness of the X-ray emission line from neutral iron, which likely originates in the illuminated torus, of objects with high Eddington ratios ([5]).

Super-Eddington accretion rates cause another influence upon the NIR flux. When the accretion rate becomes super-Eddington, the disk self-gravity starts to govern the disk and truncate the outer part of the disk. Due to the truncation, super-Eddington disks do not radiate at NIR ([20]).

In contrast to the result for a thin disk with a sub-Eddington accretion rate, a super-Eddington accretion rate leads to a much weaker NIR emission because of the two effects above. In other words, object selections with rest-NIR emission tend to miss super-Eddington accretors.

4.3 Summary and prospects

We have investigated the consequences of the anisotropic nature of the disk emission ([18], [19]). We found that the torus inner region is much close to the disk and concave. Also, the anisotropy naturally resolves the conflict in the NIR time delay – luminosity relation between theory and observations. Larger inclination angles (corresponding to intermediate type-1 AGNs, such as type 1.9) lead to longer time delays. Large accretion rates result in the weak NIR emission, due to the large disk shade and the disk truncation. Therefore, we tend to miss super-Eddington accretors when we include the NIR flux to select objects from survey

data. More predictions for other quantities (such as variability amplitudes) and for other dependencies (torus thickness and torus-disk misalignment) are presented in [19].

Now, we mention the prospects for future X-ray mission Astro-H, which will have a high spectral resolution of the order of 100km/s. Figure 2 shows the expected velocity of clumps in the torus by various colors. At the inner edge of the torus, clumps will have velocity dispersion of $\sim 1500 - 3000$ km/s. Thus, such clump kinematics will be unveiled by Astro-H.

References

- [1] Abramowicz, M. A., Czerny, B., Lasota, J. P., & Szuszkiewicz, E. 1988, *ApJ*, 332, 646
- [2] Antonucci, R. 1993, *ARAA*, 31, 473
- [3] Antonucci, R. R. J., & Miller, J. S. 1985, *ApJ*, 297, 621
- [4] Barvainis, R. 1987, *ApJ*, 320, 537
- [5] Bianchi, S., Guainazzi, M., Matt, G., & Fonseca Bonilla, N. 2007, *A&A*, 467, L19
- [6] Clavel, J., Wamsteker, W., & Glass, I. S. 1989, *ApJ*, 337, 236
- [7] Collin, S., & Kawaguchi, T. 2004, *A&A*, 426, 797
- [8] Efstathiou, A., & Rowan-Robinson, M. 1995, *MNRAS*, 273, 649
- [9] Fukue, J. 2000, *PASJ*, 52, 829
- [10] Fukue, J., & Sanbuichi, K. 1993, *PASJ*, 45, 135
- [11] Granato, G. L., & Danese, L. 1994, *MNRAS*, 268, 235
- [12] Glass, I. S. 1992, *MNRAS*, 256, 23P
- [13] Glass, I. S. 2004, *MNRAS*, 350, 1049
- [14] Hao, H., et al. 2010, *ApJL*, 724, L59
- [15] Hönig, S. F., & Beckert, T. 2007, *MNRAS*, 380, 1172
- [16] Jiang, L., et al. 2010, *Nature*, 464, 380
- [17] Kawaguchi, T. 2003, *ApJ*, 593, 69
- [18] Kawaguchi, T., & Mori, M. 2010, *ApJL*, 724, L183
- [19] Kawaguchi, T., & Mori, M. 2010, *ApJ*, 737, 105
- [20] Kawaguchi, T., Pierens, A., & Huré, J.-M. 2004, *A&A*, 415, 47
- [21] Kishimoto, M., Hönig, S. F., Beckert, T., & Weigelt, G. 2007, *A&A*, 476, 713
- [22] Krolik, J., & Begelman, M. C. 1988, *ApJ*, 329, 702
- [23] Laor, A., & Netzer, H. 1989, *MNRAS*, 238, 897
- [24] Minezaki, T., Yoshii, Y., Kobayashi, Y., Enya, K., Suganuma, M., Tomita, H., Aoki, T., & Peterson, B. A. 2004, *ApJL*, 600, L35
- [25] Nelson, B. O. 1996, *ApJL*, 465, L87
- [26] M. M., Nikutta, R., Ivezić, Ž., & Elitzur, M. 2008, *ApJ*, 685, 160

- [27] Oknyanskij, V. L., & Horne, K. 2001, *Probing the Physics of Active Galactic Nuclei*, 224, 149
- [28] Oknyanskij, V. L., Lyuty, V. M., Taranova, O. G., & Shenavrin, V. I. 1999, *Astronomy Letters*, 25, 483
- [29] Pier, E. A., & Krolik, J. H. 1992, *ApJ*, 401, 99
- [30] Pier, E. A., & Krolik, J. H. 1993, *ApJ*, 418, 673
- [31] Pogge, R. W. 1989, *ApJ*, 345, 730
- [32] Rodríguez-Ardila, A., & Mazzalay, X. 2006, *MNRAS*, 367, L57
- [33] Schmitt, H. R., & Kinney, A. L. 1996, *ApJ*, 463, 498
- [34] Sun, W.-H., & Malkan, M. A. 1989, *ApJ*, 346, 68
- [35] Suganuma, M., et al. 2004, *ApJL*, 612, L113
- [36] Suganuma, M., et al. 2006, *ApJ*, 639, 46
- [37] Telesco, C. M., Becklin, E. E., Wynn-Williams, C. G., & Harper, D. A. 1984, *ApJ*, 282, 427
- [38] Vollmer, B., Beckert, T., & Duschl, W. J. 2004, *A&A*, 413, 949
- [39] Wilson, A. S., & Tsvetanov, Z. I. 1994, *AJ*, 107, 1227